Master of Science

Prediction of Behind-Iris Structures by Use of Anterior Segment Optical Coherence Tomography Parameters

The Graduate School

of the University of Ulsan

Department of Medicine

Yeji Moon

Prediction of Behind-Iris Structures by Use of Anterior Segment Optical Coherence Tomography Parameters

Supervisor : Kyung Rim Sung

A dissertation

Submitted to

The Graduate School of the University of Ulsan

In partial Fulfillment of the Requirements

For the Degree of

Master of Science

By

Yeji Moon

Department of Medicine

Ulsan, Korea

February 2018

Prediction of Behind-Iris Structures by Use of Anterior Segment Optical Coherence Tomography Parameters

This certifies that the dissertation

of Yeji Moon is approved.

Jae Yong Kim

Committee Chair Dr.

Kyung Rim Sung

Committee Member Dr.

Joo Yong Lee

Committee Member Dr.

Department of Medicine

Ulsan, Korea

February 2018

Prediction of Behind-Iris Structures by Use of Anterior Segment Optical Coherence Tomography Parameters

Purpose: To evaluate whether the ultrasound biomicroscopy (UBM) parameters associated with structures behind iris can be induced using anterior segment optical coherence tomography (AS OCT) parameters in patients with primary angle closure (PAC).

Study design: Retrospective, observational study

Subjects: A total of 106 eyes of 106 PAC patients

Methods: PAC eyes were imaged using both UBM and AS OCT under the same lighting conditions. Anterior chamber depth, anterior chamber area, lens vault, iris cross-sectional area, iris curvature, iris thickness at 750μm form the scleral spur (SS), angle-opening distance at 750μm anterior to SS, angel recess area at 750μm anterior to SS, trabecular iris space area at 750μm anterior to SS, and pupil diameter were estimated on AS OCT image; trabecular-ciliary process angle, trabecular-ciliary process distance, iris-ciliary process distance, ciliary body thickness 1mm posterior to SS were measured on UBM image using ImageJ software. UBM images were categorized into one of three angle closure mechanisms; pupillary block (PB), plateau iris configuration (PIC), and iridolenticular wrapping (WR).

Outcome measure: Uni- and multivariate linear regression analysis were used for prediction of UBM parameters. Subgroup comparison was done with Kruskal-Wallis test, χ^2-test and Mann-Whitney test.

Results: Forty-nine eyes were categorized into PB group, 28 eyes into PIC group, and 29 eyes into WR group. In multivariate linear regression, LV, IC and IA were major parameters to predict behind-iris structure. Coefficients of determination of multivariate linear regression analysis for UBM parameter were 3.9~28.3%. PB group showed larger IC compared with the other groups. AOD750 in PIC group was longer than those in the other groups, and WR group had smaller ACD and larger LV compared with the other groups.

Conclusions: AS OCT parameters alone are insufficient to predict and explain the UBM parameters. However, some AS OCT parameters are associated with subclassification using

UBM images showing behind-iris structures, thus angle closure mechanism classification can be done by assist of AS OCT parameters.

Keywords : Primary angle closure (PAC), anterior segment optical coherence tomography (AS OCT), ultrasound biomicroscopy (UBM)

Index

Table & Figure index

Introduction

Primary angle closure glaucoma (PACG) is one of the major causes of blindness.[1-4] Primary angle closure (PAC) is principally caused by pupillary block (PB). In pupillary block, the aqueous flow from the posterior chamber, where it is produced by the nonpigmented ciliary epithelium, to the anterior chamber (AC) is limited in the region of iridolenticular contact. Accordingly, laser peripheral iridotomy (LPI) is the primary treatment option for the management of PAC, as it eliminates pupillary block and makes new shunt of aqueous flow.[5-8] However, the AC angles of some PAC eyes with patent LPI showed progression of peripheral anterior synechiae (PAS), persistent angle closure and an increased intraocular pressure (IOP).[9-14] Therefore, several investigators have raised some suggestion that other pathogenic mechanisms contribute to PAC such as plateau iris configuration (PIC), iridolenticular wrapping (WR).[15-20]

Some researchers have attempted to categorized PAC into subgroups using anterior segment optical coherence tomography (AS OCT) images.[21-23] Although gonioscopic examination is regarded as the gold standard for angle evaluation, it is a subjective technique and difficult to quantify.[24] AS OCT is a device that can acquire an anterior segment image with high resolution and allow an objective, reproducible, and quantitative assessment of the anterior segment including the angle by noncontact method with the patient in a sitting position. Also it is easy to use after minimal training.[25-27]

However, it is hard to determine the PAC mechanisms using only AS OCT which cannot visualize the structure behind the iris such as ciliary body (CB), sulcus or peripheral lens. With ultrasound biomicroscopy (UBM), it is possible to visualize the structure behind the iris.[28]

Thus in this study, we aimed to evaluate whether the UBM parameters associated with structure behind iris could be induced using AS OCT parameters in PAC and PACG patients. In addition, we intended to compare AS OCT parameter in subgroup which was classified with UBM imaging.

Patients and Methods

Subjects

PAC or PACG patients who were examined by a single glaucoma specialist (K.R.S) at the glaucoma clinic of University of Ulsan College of Medicine, Asan Medical Center, Seoul, Korea and who met the inclusion criteria were included based on medical record review. We pooled both PAC and PACG eyes and defined them as "angle closure" in our current study. The study was approved by the Institutional Review Board of Asan Medical Center, and we followed the tenets of the Declaration of Helsinki.

All participants underwent complete ophthalmic examinations, including medical history review, best corrected visual acuity (BCVA), slit-lamp biomicroscopy, Goldmann applanation tonometry (GAT), gonioscopy, funduscopic examination using a 90- or 78-diopter lens, stereoscopoic optic disc photography, central corneal thickness (CCT) by DGH-550 instrument (DGH Technology Inc., Exton, PA), retinal nerve fiber layer photography, visual field (VF) test (Humphrey field analyzer, Swedish Interactive Threshold Algorithm (SITA) 24-2; Carl Zeiss Meditec, Dublin, CA), axial length (AXL) by partial coherence interferometer (IOLMaster; Carl Zeiss Meditec Inc.), UBM (HiScan; Optikon, Rome, Italy), and AS OCT (Visante OCT, ver. 2.0; Carl Zeiss Meditec).

PAC and PACG were diagnosed by gonioscopic examination. PAC was diagnosed when an eye had an occludable angle (appositional contact between the peripheral iris and the posterior trabecular meshwork on non-indentation gonioscopy for at least 180° in primary position) and exhibited features indicative of trabecular obstruction by the peripheral iris, such as elevated IOP, the presence of PAS, iris whorling, "glaukomflecken" lens opacity, or excessive pigment deposition on the trabeculr surface, but without the development of a glaucomatous optic disc or any VF change.[18,23,29] PAC with glaucomatous optic disc changes (neuroretinal rim thinning, disc excavation, or optic disc hemorrhage attributable to glaucoma) or a glaucomatous VF change (pattern standard deviation < 5% and values outside the normal limits on the glaucoma hemifield test) were diagnosed as PACG.

We excluded patients with history or current use of topical or systemic medications that might have affected the angle or the pupillary reflex, those with history of previous

intraocular surgery including cataract surgery, laser trabeculoplasty, laser iridoplasty, and those who were unable to fixate prior to the AS OCT examination. Patients with a history of acute PAC (defined by the presence of ocular or periocular pain, nausea, or vomiting, and a history of intermittent blurring of vision with haloes; a presenting IOP >30mmHg on GAT; and the presence of at least three of the following signs: conjunctival injection, corneal epithelial edema, mid-dilated unreactive pupil, and shallow AC) were also excluded. Eyes with secondary angle closure, such as neovascular or uveitic glaucoma, were also excluded. Patients who had duration longer than 1year between AS OCT and UBM imaging or those who had laser LPI between two imaging tests were excluded.

Slit Lamp Examination and Gonioscopy

Before AS OCT imaging, all subjects underwent slit lamp biomicroscopy and gonioscopy by an independent observer (K.R.S) with extensive experience in performing gonioscopy. All eyes were examined with a Sussman 4-mirror lens (Ocular Instruments, Bellevue, WA) under the room light (0.5cd/m^2). Both static and dynamic gonioscopies were performed with the eye in the primary position. Indentation gonioscopy was performed to determine whether angle closure was attributable to PAS. Care was taken to ensure that light did not fall on the pupil during the examinations to avoid miosis.

Anterior Segment Optical Coherence Tomography and Ultrasound Biomicroscopy Imaging

All subjects were imaged in terms of the nasal and temporal angles (0°-180°) using AS OCT operating in the enhanced AS single mode (scan length 16mm; 256 A-scans). UBM was conducted under topical anesthesia using 0.5% proparacaine (Alcaine; Alcon Laboratories, Inc., Fort Worth, TX). An eyecup was used dependent on the ocular aperture size, and it was filled with sterile normal saline. The patient was then asked to fixate on a ceiling target; the fellow eye was used to maintain accommodation and fixation. The UBM device was equipped with a 35-MHz transducer, which had a wide-view probe that enabled up to 70um of axial and lateral resolution in the AS, with a penetration of 7 to 8 mm. Cross-sectional images were obtained from the nasal, temporal, superior and inferior angles (0°-

90°-180°-270°). All images were obtained under the same light condition (3.25cd/m^2) by a single, well-trained operator.

Image Analysis

A single examiner (Y.M.), who was blinded to the other test results and all clinical data of the participants evaluated all images. If both eyes met the including criteria, one eye was randomly chosen. To compare the structure in AS OCT and UBM image, temporal side images were evaluated in this study. Anterior chamber depth (ACD), angle-opening distance at 750μm anterior to scleral spur (AOD750), angel recess area at 750μm anterior to scleral spur (ARA750), trabecular iris space area at 750μm anterior to scleral spur (TISA750), and lens vault (LV) were measured by the in-built software of AS OCT. In the AS OCT image, pupil diameter (PD), iris cross-sectional area (IA), iris thickness 750μm form the scleral spur (IT750), iris curvature (IC), and anterior chamber area (AA) were measured using ImageJ software (version 1.51; Wayne Rasband, National Institutes of Health, Rockville, MD) (Figure 1). Likewise, UBM parameters including trabecular-ciliary process angle (TCA), trabecular-ciliary process distance (TCPD), iris-ciliary process distance (ICPD), and CB thickness 1mm posterior to the scleral spur (CBT1) were measured (Figure 2). Parameter measurement procedure has been described in detail elsewhere.[13,30-32]

In AS OCT image, ACD was defined as the distance from the corneal endothelium to the anterior surface of the lens. The scleral spur (SS) was defined as the point at which a change in curvature of the inner surface of the angle wall became apparent, and often presented as an inward protrusion of the sclera.[33] After determination of the SS location, IT750 was measured.[31-35] IA was defined as the cross-sectional area of temporal side. AA was defined as the cross-sectional area bordered at corneal endothelium and anterior surface of lens and iris. IC was defined as the maximum perpendicular distance between the iris pigment epithelium and the line connecting the most peripheral to the most central point of the epithelium.[34] The LV was defined as perpendicular distance between the anterior pole of the crystalline lens and the horizontal line joining the two SSs.[18,35]

TCPD was measured on a line extending from the corneal endothelium 500mm form the

SS perpendicularly through the posterior surface of iris to the ciliary process. ICPD was measured from the posterior iris surface to the ciliary process along the same line as TCPD. TCA was measured with the SS as the apex, the corneal endothelium and the superior surface of ciliary process as the arms of the angle.[36,37]

Quantitative parameters measured using ImageJ software were averaged from repeated measurement which were performed twice independently. The intraclass coefficient values of the parameters were between 0.921 and 0.958.

Subgroup Classification

UBM images were categorized into one of three angle closure mechanisms: pupillary block (PB), plateau iris configuration (PIC), iridolenticular wrapping (WR). When the image suggested multiple mechanisms for angle closure, one examiner (Y.M.) selected the dominant mechanism without other clinical information.

The guidelines to classify the UBM images into three mechanisms were (1) PB: convex iris configuration with decreased iridolenticular contact (2) PIC: anteriorly directed ciliary body, absent ciliary sulcus, steep iris approach from its point of insertion followed by a downward angulation from the corneoscleral wall, and presence of a central flat iris plane (3) WR: shallow central and peripheral anterior chamber depth, and increased iridolenticular contact distance (Figure 3).[20]

Statistical Analysis

Uni- and multivariate regression analysis were performed to evaluate the association between parameters of two imaging devices. Variables with a probability value ≤ 0.20 in univariate analyses were included in the multivariate analysis. The 1-sample Kolmogorov-Smirnov test was used to evaluate normality of the parameters in each subgroup. The AC parameters between subgroups were compared using Kruskal-Wallis test, χ^2-test and Mann-Whitney test as a post-hoc analysis. All statistical analyses were performed using SPSS program (version 21.0; SPSS Inc., Chicago, IL).

Result

Subjects Characteristics

A total of 124 eyes of 124 angle closure subjects were eligible for initial inclusion criteria; among them, 18 eyes (14.5%) were excluded due to poor UBM image. Thus, 106 eyes from 106 patients with PAC or PACG were included in final analysis. The patients' mean age was 65.1±8.7 years; 15 were men, 91 were women, and all were Korean. Forty-nine patients were diagnosed as PAC and 57 were PACG; 50 right eyes and 56 left eyes were included. Finally, 49 eyes were categorized into PB group, 28 eyes into PIC group, and 29 eyes into WR group as dominant angle closure mechanism.

The demographic and ocular biometric data with each angle closure mechanism are shown in Table 1. There was no significant difference in age, sex, BCVA, spherical equivalent, IOP, CCT, AXL, and PD among the three subgroups.

Prediction of Behind-Iris Structure

Tables 2-6 showed prediction of UBM parameters related to behind-iris structure with AS OCT parameters using uni- and multivariate linear regression. LV, IC, and IA were major parameters to predict behind-iris structure.

TCA had only one variable in multivariate linear regression, and TCPD had two variables. The coefficients of determination (R^2) of multivariate linear regression analysis for TCA and TCPD were about 5% (Table 7). The equation of multivariate linear regression for ICPD/TCPD ratio showed highest R^2 (28.3%). While LV and IC showed positive slopes, IA had a negative slope in the equations.

Comparison of AS OCT Parameters among the Subgroups

In Kruskal-Wallis test and post-hoc analysis, PB group showed large IC compared with the other groups. AOD750 in PIC group was longer than those in the other groups. WR group had small ACD and large LV compared with the other groups. Statistically significant difference of AA showed between PIC and WR groups (Table 8, Figure 4).

Discussion

Currently, it is generally accepted that angle closure is not caused by a simple anatomical condition or a single mechanism, but contributed by multiple mechanisms. Pupillary block may be one of the major mechanisms, and LPI is recommended for most angle closure patients. However, plateau iris configuration or forward movement of lens may play more important role in some patients. Therefore, the categorization of angle closure eyes according to difference in mechanisms is important, because the treatment may vary in different mechanisms.[17,18,38]

In the previous reports, we showed 2 clusters according to the AS OCT parameters and/or the UBM parameters.[21,22,39] Unlike the previous reports, in present study we categorized the subjects into the three subgroups according to the UBM imaging before the AS OCT parameters analysis. We decided to set three group, not two group (PB vs non-PB), to categorize the subjects more specifically.

In previous study, we showed one cluster with low IC in AS OCT, small TCA and TCPD in UBM, and low IOP reduction after LPI, which implied PIC.[39] In another study, one cluster had features including high ACD and long AOD750, low LV and small change in AOD750 after LPI, which also implied PIC.[22] In present study, as mentioned above, we classified some subjects into the PIC group according to the UBM image. The results that PIC group featured higher ACD and AA, lower LV and IC, greater AOD750 supported the result of the previous analysis.

In multivariate linear analysis to predict the UBM parameters, coefficients of determination were smaller than 0.3 in general. This means that the AS OCT parameters alone are insufficient to predict and explain the UBM parameters. There are several reasons for this. First, AS OCT parameters other than the parameters that we currently use may be needed to predict UBM parameters. Second, the non-linear regression in modeling the UBM parameters may be considered. Third, there are some limits of accuracy for the image acquisition and parameters measurement. Last, the possibility of other factors besides the parameters on the AS OCT image may be considered.

However, even though it is difficult to predict the UBM parameters specifically, there are

AS OCT parameters that show statistically significant differences for each mechanism, thus it can help to classify the angle closure. Figure 5 shows the distribution of subjects according to IC, AOD750, and LV. Although it is difficult to present a cut-off value that is the basis of classification in this study, it is expected that a more elaborate classification guideline can be presented if more patients are analyzed.

Our study has several limitations. First, UBM has lower resolution than newly developed high-resolution AS OCT. In addition, UBM is more dependent to operator. Therefore we had to exclude poor-quality UBM images which may affect the outcomes. Nonetheless, we had some limitations of imaging analysis; for example ciliary process overlapping with iris. To overcome this limitation, we measured UBM and AS OCT parameters using ImageJ software repeatedly and averaged repeated measurements. Second, not all eyes underwent imaging before LPI, thus both pre-LPI and post-LPI eyes were included. However, all images showed cross-sectional images not including the LPI sites. Third, our subclassification of angle closure did not include all features, such as dynamic factors, because all images were acquired under the same lighting conditions. Last, pupil diameter can affect AS OCT and UBM parameters. For this reason, we measured and included pupil diameter as a covariate in the analysis.

In conclusion, AS OCT parameters alone are insufficient to predict and explain the UBM parameters. However, some AS OCT parameters are associated with subclassification using UBM images showing behind-iris structures. These observations suggested that, in clinical situation, UBM image is necessary to evaluate exactly the behind-iris structure, however angle closure mechanism classification can be done by assist of AS OCT parameters.

Reference

1. Congdon N, Wang F, Tielsch JM. Issues in the epidemiology and population-based screening of primary angle-closure glaucoma. *Surv Ophthalmol.* 1992;36:411-23.
2. Foster PJ, Baasanhu J, Alsbirk PH, et al. Glaucoma in Mongolia. A population-based survey in Hovsgol province, northern Mongolia. *Arch Ophthalmol.* 1996;114:1235-41.
3. Foster PJ, Johnson GJ. Glaucoma in China: how big is the problem? *Br J Ophthalmol.* 2001;85:1277-82.
4. Quigley HA, Broman AT. The number of people with glaucoma worldwide in 2010 and 2020. *Br J Ophthalmol.* 2006;90:262-7.
5. Snow JT. Value of prophylactic peripheral iridectomy on the second eye in angle-closure glaucoma. *Trans Ophthalmol Soc U K.* 1977;97:189-91.
6. Edwards RS. Behaviour of the fellow eye in acute angle-closure glaucoma. *Br J Ophthalmol.* 1982;66:576-9.
7. Saw SM, Gazzard G, Friedman DS. Interventions for angle-closure glaucoma: an evidence-based update. *Ophthalmology.* 2003;110:1869-78; quiz 78-9, 930.
8. Nolan WP, Foster PJ, Devereux JG, et al. YAG laser iridotomy treatment for primary angle closure in east Asian eyes. *Br J Ophthalmol.* 2000;84:1255-9.
9. Alsagoff Z, Aung T, Ang LP, et al. Long-term clinical course of primary angle-closure glaucoma in an Asian population. *Ophthalmology.* 2000;107:2300-4.
10. Ang LP, Aung T, Chew PT. Acute primary angle closure in an Asian population: long-term outcome of the fellow eye after prophylactic laser peripheral iridotomy. *Ophthalmology.* 2000;107:2092-6.
11. Aung T, Ang LP, Chan SP, et al. Acute primary angle-closure: long-term intraocular pressure outcome in Asian eyes. *Am J Ophthalmol.* 2001;131:7-12.

12. He M, Friedman DS, Ge J, et al. Laser peripheral iridotomy in primary angle-closure suspects: biometric and gonioscopic outcomes: the Liwan Eye Study. *Ophthalmology.* 2007;114:494-500.
13. Lee KS, Sung KR, Kang SY, et al. Residual anterior chamber angle closure in narrow-angle eyes following laser peripheral iridotomy: anterior segment optical coherence tomography quantitative study. *Jpn J Ophthalmol.* 2011;55:213-9.
14. Choi JS, Kim YY. Progression of peripheral anterior synechiae after laser iridotomy. *Am J Ophthalmol.* 2005;140:1125-7.
15. He M, Foster PJ, Johnson GJ, et al. Angle-closure glaucoma in East Asian and European people. Different diseases? *Eye (Lond).* 2006;20:3-12.
16. Kumar RS, Baskaran M, Chew PT, et al. Prevalence of plateau iris in primary angle closure suspects an ultrasound biomicroscopy study. *Ophthalmology.* 2008;115:430-4.
17. Kumar RS, Tantisevi V, Wong MH, et al. Plateau iris in Asian subjects with primary angle closure glaucoma. *Arch Ophthalmol.* 2009;127:1269-72.
18. Nongpiur ME, He M, Amerasinghe N, et al. Lens vault, thickness, and position in Chinese subjects with angle closure. *Ophthalmology.* 2011;118:474-9.
19. Zhang Y, Li SZ, Li L, et al. Quantitative analysis of iris changes following mydriasis in subjects with different mechanisms of angle closure. *Invest Ophthalmol Vis Sci.* 2015;56:563-70.
20. Moghimi S, Kiaroudi M, Coh P, et al. Comparison of Anterior Chamber Parameters in Patients With Plateau Iris Configuration and Pupillary Block Using ASOCT. *J Glaucoma.* 2017;26:153-8.
21. Baek S, Sung KR, Sun JH, et al. A hierarchical cluster analysis of primary angle closure classification using anterior segment optical coherence tomography parameters. *Invest Ophthalmol Vis Sci.* 2013;54:848-53.
22. Han S, Sung KR, Lee KS, et al. Outcomes of laser peripheral iridotomy in angle closure subgroups according to anterior segment optical coherence

tomography parameters. *Invest Ophthalmol Vis Sci.* 2014;55:6795-801.

23. Nongpiur ME, Gong T, Lee HK, et al. Subgrouping of primary angle-closure suspects based on anterior segment optical coherence tomography parameters. *Ophthalmology.* 2013;120:2525-31.
24. Foster PJ, Devereux JG, Alsbirk PH, et al. Detection of gonioscopically occludable angles and primary angle closure glaucoma by estimation of limbal chamber depth in Asians: modified grading scheme. *Br J Ophthalmol.* 2000;84:186-92.
25. Kim DY, Sung KR, Kang SY, et al. Characteristics and reproducibility of anterior chamber angle assessment by anterior-segment optical coherence tomography. *Acta Ophthalmol.* 2011;89:435-41.
26. Radhakrishnan S, Goldsmith J, Huang D, et al. Comparison of optical coherence tomography and ultrasound biomicroscopy for detection of narrow anterior chamber angles. *Arch Ophthalmol.* 2005;123:1053-9.
27. Nolan WP, See JL, Chew PT, et al. Detection of primary angle closure using anterior segment optical coherence tomography in Asian eyes. *Ophthalmology.* 2007;114:33-9.
28. Blieden LS. Diagnostic Imaging of the Anterior Segment in Glaucoma: An Update. *Int Ophthalmol Clin.* 2017;57:125-36.
29. Foster PJ, Buhrmann R, Quigley HA, et al. The definition and classification of glaucoma in prevalence surveys. *Br J Ophthalmol.* 2002;86:238-42.
30. Yun SC, Hong JW, Sung KR, et al. Effects of Laser Peripheral Iridotomy in Subgroups of Primary Angle Closure Based on Iris Insertion. *J Ophthalmol.* 2015;2015:581719.
31. Lee Y, Sung KR, Na JH, et al. Dynamic changes in anterior segment (AS) parameters in eyes with primary angle closure (PAC) and PAC glaucoma and open-angle eyes assessed using AS optical coherence tomography. *Invest Ophthalmol Vis Sci.* 2012;53:693-7.
32. Sun JH, Sung KR, Yun SC, et al. Factors associated with anterior chamber narrowing with age: an optical coherence tomography study. *Invest*

Ophthalmol Vis Sci. 2012;53:2607-10.

33. Sakata LM, Lavanya R, Friedman DS, et al. Assessment of the scleral spur in anterior segment optical coherence tomography images. *Arch Ophthalmol.* 2008;126:181-5.
34. Wang B, Sakata LM, Friedman DS, et al. Quantitative iris parameters and association with narrow angles. *Ophthalmology.* 2010;117:11-7.
35. Nongpiur ME, Sakata LM, Friedman DS, et al. Novel association of smaller anterior chamber width with angle closure in Singaporeans. *Ophthalmology.* 2010;117:1967-73.
36. Mansoori T, Sarvepally VK, Balakrishna N. Plateau Iris in Primary Angle Closure Glaucoma: An Ultrasound Biomicroscopy Study. *J Glaucoma.* 2016;25:e82-6.
37. He N, Wu L, Qi M, et al. Comparison of Ciliary Body Anatomy between American Caucasians and Ethnic Chinese Using Ultrasound Biomicroscopy. *Curr Eye Res.* 2016;41:485-91.
38. Wang BS, Narayanaswamy A, Amerasinghe N, et al. Increased iris thickness and association with primary angle closure glaucoma. *Br J Ophthalmol.* 2011;95:46-50.
39. Kwon J, Sung KR, Han S, et al. Subclassification of Primary Angle Closure Using Anterior Segment Optical Coherence Tomography and Ultrasound Biomicroscopic Parameters. *Ophthalmology.* 2017;124:1039-47.

Table 1. Demographic and ocular biometric data of patients with diffenrec angle closure mechanism

	PB (n = 49)	PIC (n = 28)	WR (n = 29)	Total (n = 106)	*P* Value
Age (year, mean ± SD)	65.5 ± 8.5	62.1 ± 9.8	67.3 ± 7.1	65.1 ± 8.7	0.065*
Male : Female (%)	14.3 : 85.7	10.7 : 89.3	17.2 : 82.8	14.2 : 85.8	0.730**
PAC : PACG (%)	49.0 : 51.0	39.3 : 60.7	48.3 : 51.7	46.2 : 53.8	0.439**
Right : Left (%)	42.9 : 57.1	42.9 : 57.1	58.6 : 41.4	47.2 : 52.8	0.832**
BCVA (mean ± SD)	0.91 ± 0.14	0.89 ± 0.17	0.91 ± 0.13	0.90 ± 0.15	0.999*
IOP (mmHg, mean ± SD)	14.6 ± 2.9	14.9 ± 2.7	14.5 ± 3.3	14.7 ± 2.9	0.700*
SE (mean ± SD)	0.91 ± 1.45	0.54 ± 1.68	0.85 ± 1.14	0.76 ± 1.44	0.816*
AXL (mm, mean ± SD)	22.78 ± 0.55	22.97 ± 0.98	22.53 ± 0.52	22.77 ± 0.67	0.215*
CCT (μm, mean ± SD)	532.8 ± 34.0	536.0 ± 37.6	531.1 ± 33.8	532.9 ± 34.2	0.664*
PD‡ (mm, mean ± SD)	4.27 ± 0.92	1.34 ± 1.00	4.02 ± 0.82	1.22 ± 0.92	0.235*

AXL; axial length, BCVA; best corrected visual acuity, CCT; central corneal thickness, IOP; intraocular pressure, PAC; primary angle closure, PACG; primary angle closure glaucoma, PB; pupillary block, PD; pupil diameter, PIC; plateau iris configuration, SD; standard deviation, SE; spherical equivalent, WR; iridolenticular wrapping

*The Kruskal-Wallis test

** The χ^2-test

‡Pupil diameter was measured on the anterior segment optical coherence tomography image.

Table 2. Prediction of CBT1 by use anterior segment optical coherence tomography parameters in linear regression analysis

	Univariate		Multivariate	
	B	*P* value	*β*	*P* value
PD	0.019	0.849		
ACD	0.198	0.042	0.198	0.042
AA	0.177	0.070		
LV	-0.069	0.482		
IA	0.112	0.252		
IC	0.020	0.383		
IT750	-0.019	0.850		
AOD750	0.031	0.751		
ARA750	0.000	0.996		
TISA750	0.014	0.886		

AA; anterior chamber area, ACD; anterior chamber depth, AOD750; angle opening distance at 750μm anterior to scleral spur, ARA750; angle recession area at 750μm anterior to scleral spur, CBT1; ciliary body thickness 1mm posterior to the scleral spur, IA; iris cross-sectional area, IC; iris curvature, IT750; iris thickness at 750μm from scleral spur, LV; lens vault, PD; pupil diameter, TISA750; trabecular-iris space area at 750μm anterior to scleral spur

Table 3. Prediction of TCA by use anterior segment optical coherence tomography parameters in linear regression analysis

	Univariate		Multivariate	
	B	*P* value	*β*	*P* value
PD	-0.048	0.623		
ACD	0.123	0.208		
AA	0.080	0.413		
LV	0.090	0.357		
IA	-0.232	0.017	-0.232	0.017
IC	0.038	0.700		
IT750	-0.117	0.231		
AOD750	0.182	0.061		
ARA750	0.188	0.054		
TISA750	0.195	0.045		

AA; anterior chamber area, ACD; anterior chamber depth, AOD750; angle opening distance at 750μm anterior to scleral spur, ARA750; angle recession area at 750μm anterior to scleral spur IA; iris cross-sectional area, IC; iris curvature, IT750; iris thickness at 750μm from scleral spur, LV; lens vault, PD; pupil diameter, TISA750; trabecular-iris space area at 750μm anterior to scleral spur, TCA; trabecular-ciliary process angle

Table 4. Prediction of ICPD by use anterior segment optical coherence tomography parameters in linear regression analysis

	Univariate		Multivariate	
	B	*P* value	*β*	*P* value
PD	0.039	0.688		
ACD	-0.201	0.039		
AA	-0.157	0.108		
LV	0.214	0.028	0.390	0.002
IA	-0.197	0.043		
IC	0.347	<0.001	0.268	0.029
IT750	-0.131	0.179		
AOD750	-0.282	0.003		
ARA750	-0.206	0.034		
TISA750	-0.240	0.013		

AA; anterior chamber area, ACD; anterior chamber depth, AOD750; angle opening distance at 750μm anterior to scleral spur, ARA750; angle recession area at 750μm anterior to scleral spur IA; iris cross-sectional area, IC; iris curvature, ICPD; iris-ciliary process distance, IT750; iris thickness at 750μm from scleral spur, LV; lens vault, PD; pupil diameter, TISA750; trabecular-iris space area at 750μm anterior to scleral spur

Table 5. Prediction of TCPD by use anterior segment optical coherence tomography parameters in linear regression analysis

	Univariate		Multivariate	
	B	*P* value	*β*	*P* value
PD	0.039	0.688		
ACD	-0.201	0.039		
AA	-0.157	0.108		
LV	0.214	0.028	0.390	0.002
IA	-0.197	0.043		
IC	0.347	<0.001	0.268	0.029
IT750	-0.131	0.179		
AOD750	-0.282	0.003		
ARA750	-0.206	0.034		
TISA750	-0.240	0.013		

AA; anterior chamber area, ACD; anterior chamber depth, AOD750; angle opening distance at 750μm anterior to scleral spur, ARA750; angle recession area at 750μm anterior to scleral spur IA; iris cross-sectional area, IC; iris curvature, IT750; iris thickness at 750μm from scleral spur, LV; lens vault, PD; pupil diameter, TCPD; trabecular-ciliary process distance, TISA750; trabecular-iris space area at 750μm anterior to scleral spur

Table 6. Prediction of ICPD/TCPD ratio by use anterior segment optical coherence tomography parameters in linear regression analysis

	Univariate		Multivariate	
	B	*P* value	*β*	*P* value
PD	0.084	0.393		
ACD	-0.277	0.004		
AA	-0.231	0.017		
LV	0.227	0.019	0.329	0.008
IA	-0.231	0.017	-0.271	0.026
IC	0.370	0.000	0.324	0.007
IT750	-0.129	0.188		
AOD750	-0.316	0.001		
ARA750	-0.228	0.019		
TISA750	-0.274	0.005		

AA; anterior chamber area, ACD; anterior chamber depth, AOD750; angle opening distance at 750μm anterior to scleral spur, ARA750; angle recession area at 750μm anterior to scleral spur IA; iris cross-sectional area, IC; iris curvature, ICPD; iris-ciliary process distance, IT750; iris thickness at 750μm from scleral spur, LV; lens vault, PD; pupil diameter, TCPD; trabecular-ciliary process distance, TISA750; trabecular-iris space area at 750μm anterior to scleral spur

Table 7. Predictability of behind-iris structure using anterior segment optical coherence tomography parameters

	Linear regression	R^2	*P* value
CBT1	0.198 ACD + 0.476	0.039	0.042
TCA	- 0.232 IA + 77.048	0.054	0.017
ICPD	0.390 LV + 0.121 IC + 0.006	0.198	0.002
TCPD	0.213 IC + 0.626	0.045	0.028
ICPD/TCPD ratio	0.329 LV + 0.324 IC - 0.271 IA + 0.196	0.283	<0.001

ACD; anterior chamber depth, CBT1; ciliary body thickness 1mm posterior to the scleral spur, IA; iris cross-sectional area, IC; iris curvature, ICPD; iris-ciliary process distance, LV; lens vault, TCA; trabecular-ciliary process angle, TCPD; trabecular-ciliary process distance, TISA750; trabecular-iris space area at 750μm anterior to scleral spur

Table 8. Comparison of anterior segment optical coherence tomography parameters among the subgroups

	PB (n = 49)	PIC (n = 28)	WR (n = 29)	*P* Value*
ACD (mm, mean±SD)	2.12 ± 0.30	2.26 ± 0.40	1.94 ± 0.26	**0.001**
AA (mm^2, mean±SD)	14.56 ± 2.82	16.16 ± 4.70	13.37 ± 2.15	**0.035**
LV (mm, mean±SD)	1.04 ± 0.29	0.94 ± 0.36	1.24 ± 0.34	**0.009**
IA (mm2, mean±SD)	1.47 ± 0.24	1.55 ± 0.28	1.52 ± 0.37	0.483
IC (mm, mean±SD)	0.30 ± 0.08	0.14 ± 0.07	0.15 ± 0.08	**<0.001**
IT750 (mm, mean±SD)	0.34 ± 0.08	0.36 ± 0.10	0.35 ± 0.09	0.939
AOD750 (mm, mean±SD)	0.21 ± 0.13	0.32 ± 0.17	0.21 ± 0.11	**0.001**
ARA750 (mm2, mean±SD)	0.12 ± 0.09	0.16 ± 0.10	0.12 ± 0.06	0.135
TISA750 (mm2, mean±SD)	0.10 ± 0.07	0.14 ± 0.08	0.11 ± 0.05	0.063

AA; anterior chamber area, ACD; anterior chamber depth, AOD750; angle opening distance at 750μm anterior to scleral spur, ARA750; angle recession area at 750μm anterior to scleral spur IA; iris cross-sectional area, IC; iris curvature, IT750; iris thickness at 750μm from scleral spur, LV; lens vault, PB; pupillary block, PIC; plateau iris configuration, TISA750; trabecular-iris space area at 750μm anterior to scleral spur, , WR; iridolenticular wrapping

*Kruskal-Wallis test. *P* values with statistical significance (<0.05) appear in boldface.

Figure 1. Quantitative parameters measured on the anterior segment optical coherence tomography

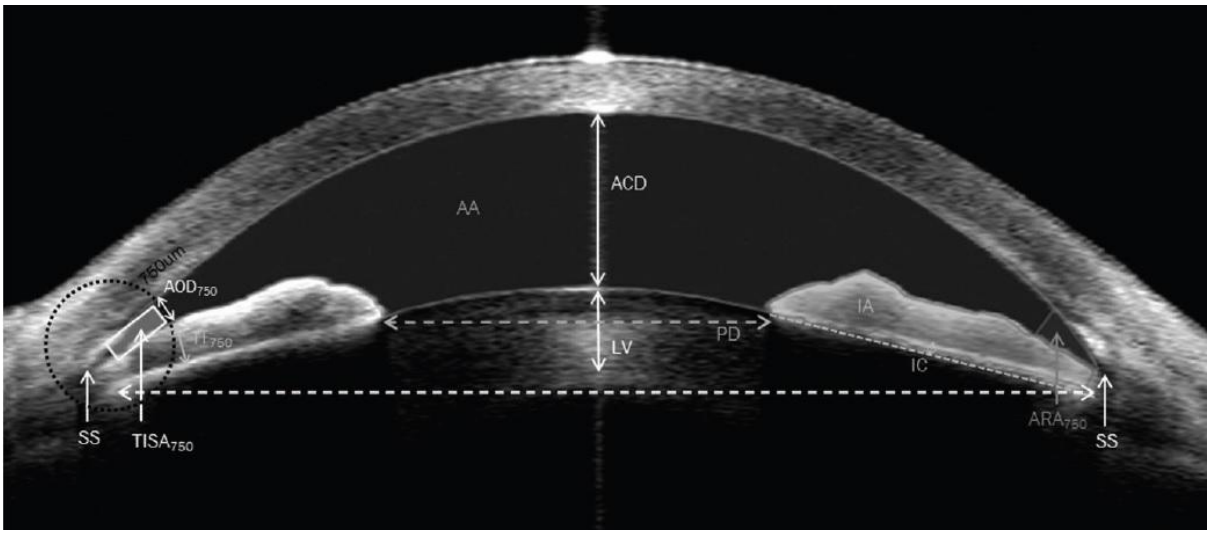

AA; anterior chamber area, ACD; anterior chamber depth, AOD750; angle opening distance at 750μm anterior to scleral spur, ARA750; angle recession area at 750μm anterior to scleral spur, IA; iris cross-sectional area, IC; iris curvature, IT750; iris thickness at 750μm from scleral spur, LV; lens vault, PD; pupil diameter, SS; scleral spur, TISA750; trabecular-iris space area at 750μm anterior to scleral spur

Figure 2. Quantitative parameters measured on the ultrasound biomicrosopic image

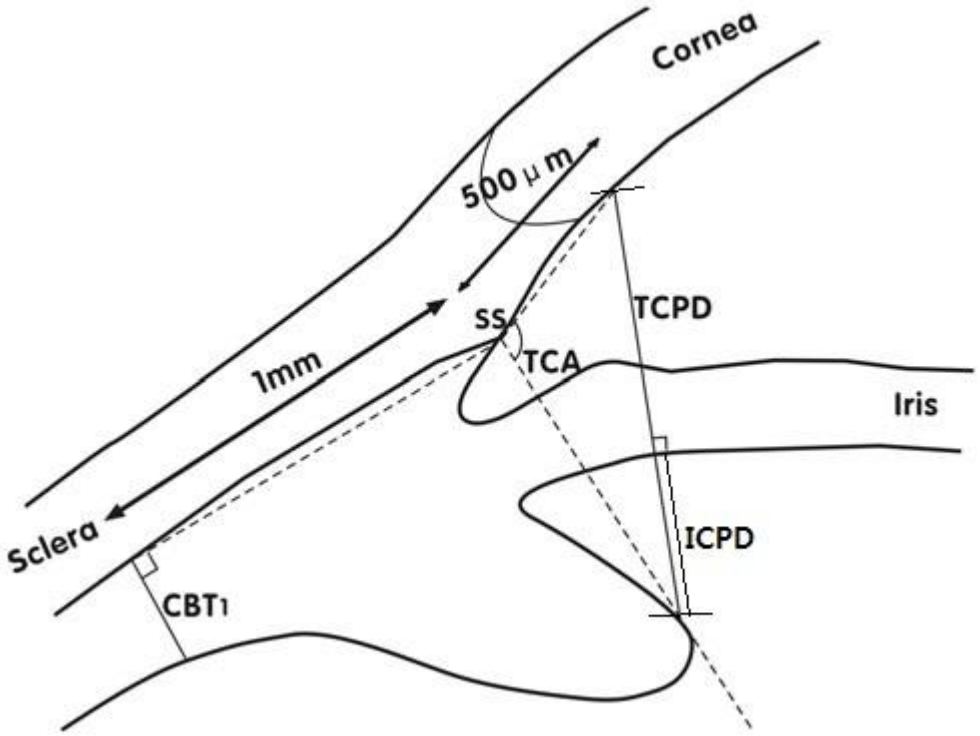

CBT1; ciliary body thickness 1mm posterior to the scleral spur, ICPD; iris-ciliary process distance, TCA; trabecular-ciliary process angle, TCPD; trabecular-ciliary process distance

Figure 3. Ultasound biomicroscopy images with different mechanisms.

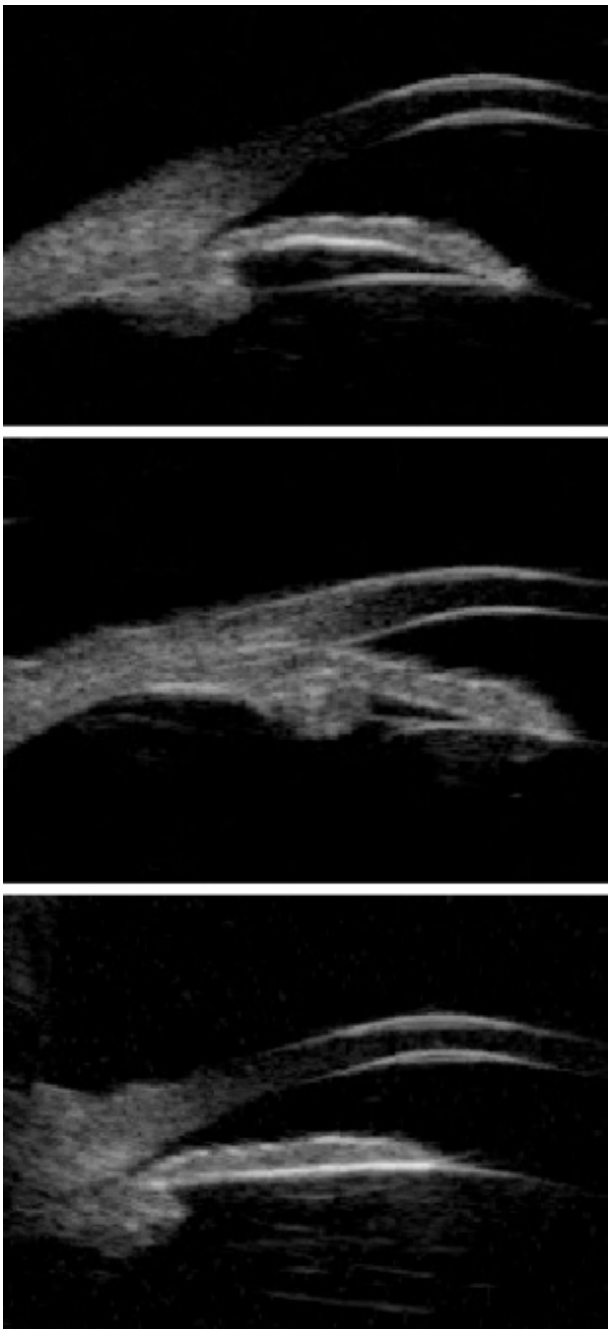

(A) pupillary block (B) plateau iris configuration (C) iridolenticular wrapping

Figure 4. Post-hoc analysis with Mann-Whitney test

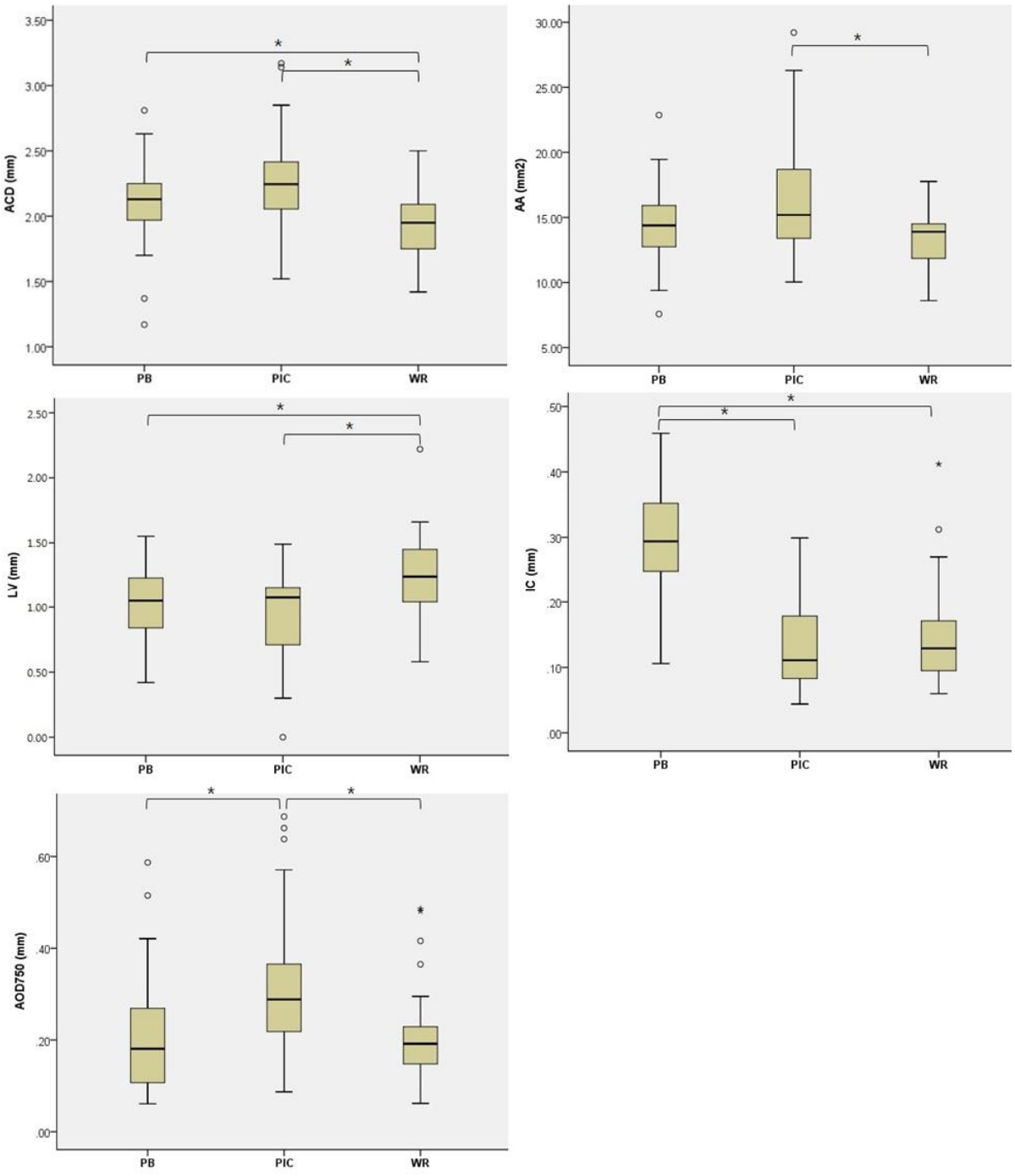

AA; anterior chamber area, ACD; anterior chamber depth, AOD750; angle opening distance at 750μm anterior to scleral spur, IC; iris curvature, LV; lens vault, PB; pupillary block, PIC; plateau iris configuration, WR; iridolenticular wrapping

*Statistically significant difference

Figure 5. The distribution of subjects according to IC, AOD750, and ACD

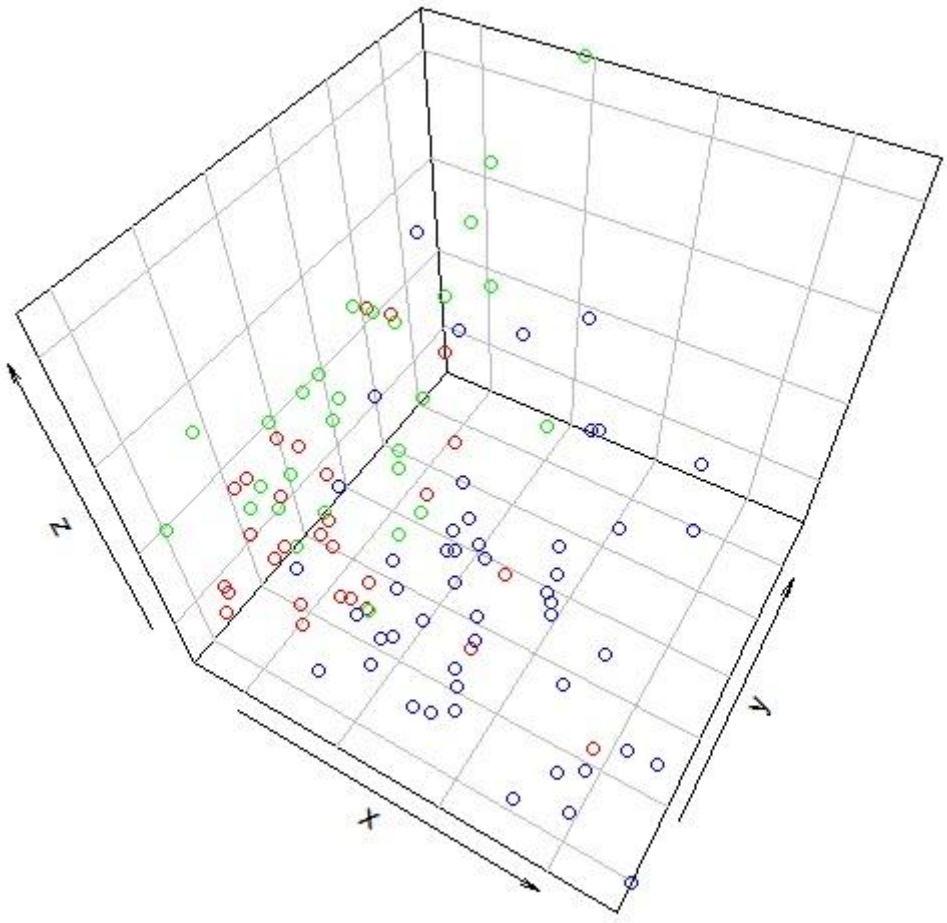

x axis: IC, *y* axis: AOD750, *z* axis : ACD

blue dot: pupillary block group, green dot: plateau iris configuration group, red dot: iridolenticular wrapping group

ACD; anterior chamber depth, AOD705; angle opening distance at 750μm anterior to scleral spur, IC; iris curvature